Available online at www.sciencedirect.com
ScienceDirect
Catalysis Today 123 (2007) 224–234
CATALYSIS TODAY
www.elsevier.com/locate/cattod

Kinetics of the water–gas shift reaction on Pt catalysts supported on alumina and ceria

A.A. Phatak [a], N. Koryabkina [b,1], S. Rai [a], J.L. Ratts [a], W. Ruettinger [c], R.J. Farrauto [c], G.E. Blau [a], W.N. Delgass [a], F.H. Ribeiro [a,*]

[a] School of Chemical Engineering, Purdue University, 480 Stadium Mall Drive, West Lafayette, IN 47907-2100, United States
[b] Department of Chemical Engineering, Worcester Polytechnic Institute, 100 Institute Road, Worcester, MA 01609-2280, United States
[c] BASF Catalysts LLC, 101 Wood Avenue, Iselin, NJ 08830, United States

Available online 9 April 2007

Abstract

We report the kinetic parameters for the water–gas shift (WGS) reaction on Pt catalysts supported on ceria and alumina under fuel reformer conditions for fuel cell applications (6.8% CO, 8.5% CO_2, 22% H_2O, 37.3% H_2, and 25.4% Ar) at a total pressure of 1 atm and in the temperature range of 180–345 °C. When ceria was used as a support, the turnover rate (TOR) for WGS was 30 times that on alumina supported Pt catalysts. The overall WGS reaction rate (r) on Pt/alumina catalysts as a function of the forward rate (r_f) was found to be: $r = r_f(1 - \beta)$, where $r_f = k_f[CO]^{0.1}[H_2O]^{1.0}[CO_2]^{-0.1}[H_2]^{-0.5}$, k_f is the forward rate constant, $\beta = ([CO_2][H_2])/(K_{eq}[CO][H_2O])$ is the approach to equilibrium, and K_{eq} is the equilibrium constant for the WGS reaction. The negative apparent reaction orders indicate inhibition of the forward rate by CO_2 and H_2. The surface is saturated with CO on Pt under reaction conditions as confirmed by diffuse reflectance infrared Fourier transform spectroscopy (DRIFTS). The small positive apparent reaction order for CO, in concert with the negative order for H_2 and the high CO coverage is explained by a decrease in the heat of adsorption as the CO coverage increases. Kinetic models based on redox-type mechanisms can explain the observed reaction kinetics and can qualitatively predict the changes in CO coverage observed in the DRIFTS study.

Keywords: Water–gas shift (WGS) reaction on Pt; Effect of ceria; Kinetics; Kinetic modeling; Design of experiments (DOE); CO heat of adsorption as a function of coverage

1. Introduction

The water–gas shift (WGS) reaction ($CO + H_2O \rightleftarrows CO_2 + H_2$) is one of the important processes used in industrial hydrogen production. Although the low temperature WGS (LT-WGS) reaction has been used in industry since the 1960s, there is renewed interest with respect to its application in fuel cell technology where a more robust catalyst is necessary. The challenge is that the CO conversion in the WGS reaction is thermodynamically more favorable at lower temperatures ($\Delta H_{298\ K} = -41.2\ kJ\ mol^{-1}$), which implies large reactor volumes unless a catalyst with a large rate per unit of volume is found. Current industrial Cu-based low temperature shift (LTS) catalysts are impractical because they require lengthy *in situ* pre-reduction, are sensitive to air (pyrophoric) and condensed water, and are poisoned by sulfur [1]. Thus, new LT-WGS catalysts, which are active and stable under the fuel processor conditions are desired. With this motivation, supported precious metal catalysts have been examined for the WGS reaction [2–6] due to their stability in air and at high temperatures, and due to their high tolerance to impurities such as sulfur [1]. Although the precious metal catalysts are more expensive and exhibit lower turnover rate than the copper-based catalysts [2], recent interest in residential and automotive fuel processor development has generated a significant drive to study supported precious metal catalysts, mainly due to their aforementioned advantages [1]. Another application of Pt catalysts is in the generation of H_2 through WGS during the short reduction cycles on lean NO_x traps for automotive applications [7]. The issues of stability during

* Corresponding author. Tel.: +1 765 494 7799; fax: +1 765 494 0805.
E-mail address: fabio@purdue.edu (F.H. Ribeiro).
[1] Current address: Solutia Inc., P.O. Box 711, Alvin, TX 77512, United States.

0920-5861/$ – see front matter © 2007 Elsevier B.V. All rights reserved.
doi:10.1016/j.cattod.2007.02.031

reduction–oxidation cycles, sulfur poisoning and high specific rates are even more critical in this application. It is necessary to understand the mechanism of the WGS reaction on supported precious metal catalysts in order to rationally improve their performance (WGS reaction rate per unit volume) through kinetic modeling.

Ceria-containing automotive three-way catalysts take advantage of the WGS reaction to reduce CO emissions [8]. The higher rates obtained by addition of ceria are an important advantage in the short contact times used in automotive applications. Gorte and co-workers [3,4] showed that the specific rate (rate per cm^2 of ceria film) of WGS on ceria-containing materials was largely independent of the nature of the precious metal but was dependent on the crystallite size of the ceria support. A bi-functional redox mechanism for the WGS reaction was suggested [3] where the ceria surface is reduced by CO spilling over from the Pt surface and this reduced ceria surface is then re-oxidized by steam. On the other hand, Shido and Iwasawa [9,10] proposed a formate mechanism to describe the WGS reaction on metal-promoted ceria. The surface formates ($HCOO_{ads}$), produced from CO reacting with active geminal surface hydroxyl (OH) groups on a partially reduced ceria surface, were suggested to be the reaction intermediate. Recently, through isotope switching experiments monitored using DRIFTS, Jacobs et al. [11,12] also observed that the mechanism over metal promoted ceria occurs through formate intermediates.

Many of the previous kinetic studies [2,3,9,10] were carried out under conditions different from the ones used in fuel processors for fuel cell applications. Under fuel cell conditions, the concentration of H_2 and CO_2 is significant (H_2 in excess) and hence in the WGS kinetic measurements it is important to study the effect of not only the reactants but also the products (H_2 and CO_2) on the forward WGS rate. For example, Koryabkina et al. [13] have found that CO_2 and H_2 inhibit the forward WGS reaction rate under fuel processing conditions for Cu-based catalysts.

The objective of this study was to determine the WGS rate, reaction orders, and activation energies on supported Pt catalysts from experiments conducted at conditions close to the ones likely to be encountered in fuel processors. We studied support effects by comparing Pt catalysts on alumina and ceria supports. We also modeled the kinetics of the WGS reaction on supported Pt catalysts by considering two mechanisms for WGS on the alumina supported catalysts: (1) redox mechanism and (2) modified redox mechanism where adsorbed CO reacts with adsorbed OH to yield CO_2 and atomic hydrogen on the surface. Diffuse reflectance infrared Fourier transform spectroscopy (DRIFTS) studies were carried out to support the kinetic modeling.

2. Experimental methods

2.1. Catalyst preparation

The 1% Pt/Al_2O_3 and 1% Pt/CeO_2 catalysts were prepared by incipient wetness impregnation of the solid support with diammineplatinum(II) nitrite $(NH_3)_2Pt(NO_2)_2$, followed by drying at 120 °C (8 h) and calcination at 500 °C (4 h) in air. The alumina support was SBA-150 (150 $m^2\ g^{-1}$) from Condea. The ceria powder was a high surface area ceria (>99%, HSA-15, ~161 $m^2\ g^{-1}$) from Rhodia. The samples were prepared using a water-based salt, which contained no chlorine or alkali. The samples were dried at RT and calcined at 500 °C [14].

For preparing the 1.66% Pt/Al_2O_3 catalyst, the incipient wetness impregnation method was used. The support used in this case was solid γ-Al_2O_3 (Puralox KR-160 from Sasol, BET surface area 145–175 $m^2\ g^{-1}$). It was impregnated using diammineplatinum(II) nitrite $(NH_3)_2Pt(NO_2)_2$ as the metal precursor. Following the impregnation, the catalyst was dried and calcined in a controlled manner. All calcinations had a feed of compressed air flowing at approximately 70 ml min^{-1}. During drying and calcination, the catalyst temperature was increased from room temperature to 120 °C at a rate of approximately 0.5 °C min^{-1}. The catalyst was then maintained at 120 °C for 10 h (drying), followed by a temperature ramp from 120 °C to 500 °C at a rate of approximately 0.5 °C min^{-1}. It was then allowed to cool to room temperature. After calcination, the catalyst was pressed into pellets, ground, and meshed in order to get a particle size in the range of 100–200 μm before loading into the reactors (to avoid excess pressure drop). It was then reduced inside the reactor under the following temperature profile. The catalyst was heated from room temperature to 350 °C at a rate of 5 °C min^{-1} in a 25% H_2/Ar mixture and kept at the final temperature for a period of 2 h.

2.2. Catalyst characterization

The Pt dispersion was determined by using the hydrogen–oxygen titration method [15,16] for alumina-supported catalysts and CO pulse chemisorption for 1% Pt/CeO_2 catalysts [17].

2.3. Kinetic measurements

2.3.1. Well-mixed reactor

The kinetic measurements were conducted at ambient pressure, in the temperature range of 180–270 °C in a well-mixed, continuous, stirred tank reactor (CSTR). A circulation pump (Senior Flexonics model MB-21HT) with a nominal air flow of 2 l min^{-1} was used for mixing. The entire setup was housed in a forced air circulation oven maintained at 130 °C. The total inlet flow rate was 118 ml min^{-1}, with an inlet gas composition of 6.8% CO, 8.5% CO_2, 22% H_2O, 37.3% H_2, and 25.4% Ar. Argon was used as an internal standard. The gases were fed to the reactor by mass flow controllers. Deionized water was metered by a water pump (Fluid Metering Inc., model QVG50) and was vaporized before entering the reactor loop. To avoid fluctuations in the water partial pressure, a 1.59 mm diameter capillary tube with the internal diameter 0.254 mm was used to deliver the water. Carbon monoxide was purified by passing it over a Cu-wire at 320 °C. Hydrogen was passed through a Deoxo trap (to remove O_2 and CO_2) and was used without further pretreatment. The gas stream was

continuously analyzed by a mass spectrometer, SRS RGA 200, and injected periodically in a gas chromatograph, HP5890, equipped with a TCD detector and a Carboxen 1000 column. Before the gas chromatograph, a condenser chilled the gases to 0 °C to maintain a low and constant amount of water. Rates were calculated from the CO and CO_2 concentrations, and the error in mass balance on carbon was less than 1%. In all cases, the rates were stable and reproducible.

We used a well-mixed differential reactor for the measurements to keep the kinetic analysis simpler and we minimized the heat and mass transfer limitations by maintaining high circulation rates. We worked in the region where the Arrhenius plot was linear (kinetically controlled regime) and avoided the conditions under which transport may start controlling the rate (observed by a change in slope). In general, to determine the reaction order of a compound, its concentration is varied while keeping the concentrations of other components constant. However, we point out that because we worked in the concentration range where the concentrations of reactants and products were significant, we could not keep the concentrations constant by using a large excess of all compounds. Thus, when the reaction order of a reactant was determined by varying its concentration, the concentration of the remaining reactants could not be kept constant. An iterative fitting correction was applied to the data to calculate reaction orders [13]. The total flow rate was maintained constant by adjusting the Ar flow rate.

We have estimated the accuracy of our measurements by carrying out multiple experiments. For the rates per gram of catalyst, we found about 20% variation in the measured values, probably due to non-uniform metal distribution in the pellets. The apparent activation energies could be reproduced within 5% and the reaction orders within 10%.

2.3.2. Tubular reactor unit

This unit consists of a plug flow reactor (PFR) housed inside a tubular furnace in order to control the temperature. The total inlet flow rate was held constant at 82.6 ml min^{-1}, with an average inlet gas composition around standard conditions as mentioned earlier. Argon was used as an internal standard. The gases were fed to the reactor using mass flow controllers. The remaining setup (e.g. water pump, gas chromatograph, water condenser) was the same one used for the well-mixed reactor. Carbon monoxide was preheated to 300 °C on a trap filled with Cu turnings before entering the reactor in order to decompose the iron carbonyls, which can otherwise deposit on the catalyst surface thereby affecting the measured rates. Carbon dioxide and hydrogen were used without any pretreatment. Rates were calculated from CO concentrations and the carbon mass balance was better than 10%. Conversion values were also recorded while performing these experiments so that the reactor could be defined either as a differential or integral reactor. In all cases, the rates were stable and reproducible.

The sequence of experiments was selected by a modified central composite design [18]. In a central composite design, all five factors (temperature and concentrations of CO, CO_2, H_2, and H_2O) can be varied simultaneously, which allows the kinetic model to capture any interactions between the parameters. In our design, we did not vary temperatures randomly because there is a longer stabilization time for the temperature to reach steady state as compared to the other factors. Due to this experimental limitation, this design was applied at two different temperatures (285 °C and 300 °C) while the remaining four factors were varied simultaneously. In addition, the temperature was varied over 255–316 °C while keeping the gas concentrations at standard conditions to determine the apparent activation energy. This design was also modified to accommodate a one-at-a-time variation approach to measure extreme points around the base or center point. The complete design consisted of a total of 284 experiments (each experiment was repeated once) and the four concentrations were varied over the ranges 4–21% CO, 5–25% CO_2, 11–34% H_2O, and 14–55% H_2. There were 19 repeat points each at approximately the center of these ranges (6.8% CO, 8.5% CO_2, 22% H_2O, and 37.3% H_2) at temperatures of 285 °C and 300 °C. By placing the center points at constant time intervals throughout the experiments, it was possible to examine the reproducibility as well as to monitor the catalyst deactivation over the duration of the experimental program. Before starting the experimental program, the catalyst was stabilized by exposing it to standard conditions (center point mentioned above) but at a temperature higher than the maximum temperature used in the designed experiments for about 8 h. We still observed deactivation during the experiments and it was a function of gas concentration and temperature. The data were corrected by assuming a linear deactivation profile between the center points (repeats). Care was taken to ensure that these statistically designed experiments remained in the differential reactor regime.

2.4. DRIFTS study of Pt/Al_2O_3 catalysts

2.4.1. DRIFTS setup

Diffuse reflectance FTIR data was collected with a Thermo Spectra-Tech Collector II DRIFTS accessory augmented with the high temperature/high pressure chamber. All the spectra were taken on a Nicolet Magna 550 FTIR using the data collection/manipulation software Omnic v7.2a at a resolution of 4 cm^{-1}. The spectra were obtained by averaging over 32 scans. The data were presented in the form of (Schuster)–Kubelka–Munk remission function (F) [19,20] as follows:

$$F(R_\infty) = \frac{(1 - R_\infty)^2}{2R_\infty} = \frac{K}{S}$$

where R_∞ is the reflectance of an ''infinitely'' thick sample (in this case, the experimentally observed reflectance), K is the molar absorption coefficient, and S is the scattering coefficient. R_∞ is experimentally defined as follows:

$$R_\infty = \frac{I_{\infty,S}}{I_{\infty,R}}$$

where $I_{\infty,S}$ is the intensity of the diffusely reflected radiation of the sample and $I_{\infty,R}$ is the intensity of the diffusely reflected radiation of the reference. In this study, $I_{\infty,R}$ was defined as the

diffusely reflected radiation of the pure catalyst at the reaction temperature prior to being exposed to the reaction gas mixture. Integrations of the FTIR peaks were completed with CasaXPS v2.3.12 software modified to process FTIR spectra.

The gas flows of N_2, CO, CO_2, and H_2 were controlled by Porter model 201 mass flow controllers. The water vapor was added to the reactant stream through a bubble gas-saturator. The saturator was heated to the temperature at which the water vapor pressure gave the desired percentage compared to atmospheric conditions. Nitrogen was then bubbled through the saturator to carry the water vapor and was mixed with the reactant stream before entering the reaction chamber. Approximately 10 mg of the 1.66% Pt/Al_2O_3 catalyst was loaded into the sample cup and the total flow was regulated at 50 sccm. Whenever water vapor was added, the nitrogen flow through the saturator was maintained at 10 sccm. All gas compositions were determined on a sccm volumetric flow rate basis.

Upon loading, the catalyst was pretreated by flowing oxygen (50 sccm) over it while it was heated to 300 °C. After the catalyst reached 300 °C, oxygen flow was continued for 15 min, and then the cell was purged with N_2 for 10 min. The catalyst was then reduced with 37% H_2 in N_2 for 20 min after which H_2 was shut off and the cell was purged with N_2 for another 10 min. The catalyst was then exposed to a 5 s pulse of O_2 to remove any CO adsorbed on Pt. Finally, the catalyst was cooled to room temperature in N_2.

2.4.2. Experimental sequence

The primary objective of the DRIFTS study was to estimate the surface coverage of CO under reaction conditions. First, the saturation coverage of CO was calibrated as follows. After the pretreatment, the catalyst was heated to 150 °C and exposed to 6.8% CO in N_2. Once the spectrum had stabilized and was recorded, the CO flow was shut off and the catalyst was heated to 300 °C. The peak area from the spectrum recorded at 150 °C was used to calibrate the saturation CO coverage on the Pt surface. At 300 °C, the catalyst was first exposed to a 5 s pulse of O_2 in order to remove the CO adsorbed on Pt, followed by exposure to water vapor to obtain the reference background.

Another objective of the DRIFTS study was to investigate the effect of changes in CO and H_2 partial pressures on the spectra and to collect information about the surface species under WGS conditions. Hence, after the background collection, the catalyst was exposed to the desired WGS experimental conditions at 300 °C in the following sequence: 1—6.8% CO, 8.5% CO_2, 37.3% H_2, 22% H_2O, and balance N_2 (standard condition), 2—13.5% CO, 8.5% CO_2, 37.3% H_2, 22% H_2O, and balance N_2 (high CO), 3—2.7% CO, 8.5% CO_2, 37.3% H_2, 22% H_2O, and balance N_2 (low CO), 4—6.8% CO, 8.5% CO_2, 55.1% H_2, 22% H_2O, and balance N_2 (high H_2), and 5–6.8% CO, 8.5% CO_2, 14% H_2, 22% H_2O, and balance N_2 (low H_2). Spectrum 1, obtained under the standard conditions, was used for comparison to detect the changes in the spectrum upon exposure to CO and H_2, spectra 2–5. The CO and H_2 partial pressures were changed to examine their effect on the surface species under the reaction conditions.

The FTIR spectra (under all reaction conditions) reached steady state in 10 min. After the spectra had stabilized, all gases except water vapor were turned off and the cell was purged with N_2 for 5 min. A 5 s pulse of O_2 was then used to remove CO adsorbed on Pt. After cleaning the Pt surface, a new background was collected and the desired gas flows were turned on. This procedure was repeated until all the experiments were completed.

3. Results

3.1. Kinetic studies on supported Pt catalysts

The main objective of this study was to measure the kinetic parameters for the WGS reaction on alumina and ceria supported Pt catalysts under the conditions relevant to fuel cell applications. In Table 1 the forward WGS reaction rates at standard conditions are reported in units of per gram of catalyst, per total moles of Pt in the catalyst and as a turnover rate (molecules converted (surface Pt atom)$^{-1}$ s^{-1}). For the catalysts supported on alumina, these rates were obtained by extrapolating the Arrhenius plot to the common temperature of 200 °C. The reaction rate per total moles of Pt on Pt/CeO_2 catalyst is about 18 times higher than that on Pt/Al_2O_3 catalyst. The TOR at standard condition is 30 times higher for the 1% Pt/CeO_2 catalyst than that for the 1% Pt/Al_2O_3 catalyst (Table 1).

The apparent activation energies and reaction orders for the forward WGS reaction are presented in Table 2. To illustrate the quality of the kinetic data, the Arrhenius plot (Fig. 1) and reaction orders (Fig. 2) are shown for the 1% Pt/Al_2O_3 sample. The apparent reaction orders with respect to reactants and products were fitted to a power rate law expression [13,21] as follows:

$$r = k_f[CO]^a[CO_2]^b[H_2]^c[H_2O]^d(1-\beta)$$

where $\beta = ([CO_2][H_2])/(K_{eq}[CO][H_2O])$ is the approach to equilibrium, k_f is the forward reaction rate constant, a, b, c, d are forward reaction orders, and K_{eq} is the equilibrium constant for the WGS reaction. The values of β were usually

Table 1
Rate of reaction in various units for the conversion of CO on different catalysts at 200 °C, 1 atm total pressure, 7% CO, 8.5% CO_2, 22% H_2O, 37% H_2, and 25% Ar

	Catalysts		
	1% Pt/Al_2O_3	1.66% Pt/Al_2O_3	1% Pt/CeO_2
Rate per gram of catalyst ($\times 10^{-6}$ mol g^{-1} s^{-1})	0.03	0.04	0.59
Rate per mole of metal ($\times 10^{-4}$ mol mol^{-1} s^{-1})	6.25	7.75	116
Percentage of metal exposed	47	69	28
TOR ($\times 10^{-3}$ s^{-1})	1.3	1.1	41.4

Table 2
Summary for the kinetics for water–gas shift reaction on Pt catalysts

Catalyst	E_a (kJ mol^{-1})	Temperature[a] (°C)	Reaction order			
			CO[b]	CO_2[c]	H_2[d]	H_2O[e]
1% Pt/Al_2O_3	68[f]	285	0.06	−0.09	−0.44	1.0
1% Pt/Al_2O_3	84[g]	315	0.1	−0.07	−0.44	1.1
1.66% Pt/Al_2O_3	81	285	0.11	−0.06	−0.49	0.82
1.66% Pt/Al_2O_3	81	300	0.1	−0.08	−0.46	0.77
1% Pt/CeO_2	75	200	−0.03	−0.09	−0.38	0.44

Standard conditions were: 7% CO, 8.5% CO_2, 22% H_2O, 37% H_2 and balance Ar to maintain constant flow rate.
[a] Temperature at which the reaction order measurements were carried out.
[b] Standard conditions except CO (5–25%) and Ar (balance).
[c] Standard conditions except CO_2 (5–30%) and Ar (balance).
[d] Standard conditions except H_2 (25–60%) and Ar (balance).
[e] Standard conditions except H_2O (10–46%) and Ar (balance).
[f] Measured between temperature range of 225–285 °C.
[g] Measured between temperature range of 285–345 °C.

less than 0.1, which indicates that the reaction is carried out far from equilibrium.

3.2. DRIFTS study of the 1.66% Pt–Al_2O_3 catalyst

The DRIFTS study was employed to determine the concentration of surface intermediates on the 1.66% Pt/Al_2O_3 catalyst. After pretreatment (see Section 2), the catalyst was first exposed to 6.8% CO in N_2 at various temperatures from room temperature to 150 °C. The spectra (not shown here) obtained under these conditions showed the presence of atop CO adsorbed on Pt. A small peak corresponding to bridge-bonded CO on Pt was also observed. In the DRIFTS spectra under WGS conditions, peaks were observed in the ranges of 1350–1400 cm^{-1}, 1550–1650 cm^{-1}, 1950–2100 cm^{-1}, and 2850–3000 cm^{-1}. Based on the peaks obtained in the ranges 1350–1400 cm^{-1}, 1550–1650 cm^{-1}, and 2850–3000 cm^{-1}, we propose that bridging formate species [11,12] are present on the surface along with atop CO.

The surface coverage of CO under WGS conditions was calibrated by assuming saturation coverage for CO exposure at 150 °C. The areas under the peak in the region 1900–2200 cm^{-1}, which corresponds to CO adsorbed on Pt, were calculated for various experimental conditions. The ratio of area under this peak for a given experimental condition to the peak area obtained from CO exposure at 150 °C gives the relative coverage under that experimental condition (Fig. 3). Under WGS conditions, flow rates of CO and H_2 were varied to examine their effect on the surface coverage of CO and compared to two models to be introduced in the next section. Fig. 3 indicates that the surface coverage of CO under various reaction conditions investigated in this study is close to the saturation coverage of CO.

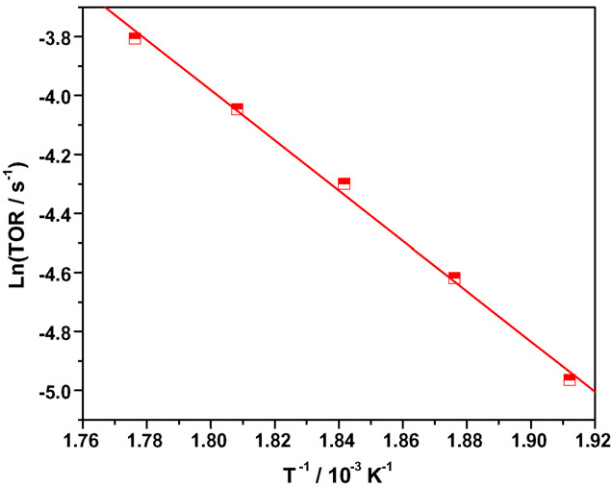

Fig. 1. Arrhenius plot for WGS in the range of 250–290 °C obtained on 1% Pt/Al_2O_3 catalyst. Inlet gas composition: 7% CO, 8.5% CO_2, 37% H_2, 22% H_2O, and 25% Ar. Total inlet flow rate of 118 ml min^{-1}.

4. Discussion

4.1. Rate of reaction and apparent activation energy

A comparison of the rates per gram of catalyst, per total moles of Pt, and TOR at standard conditions shows that Pt supported on ceria is the most active catalyst among the

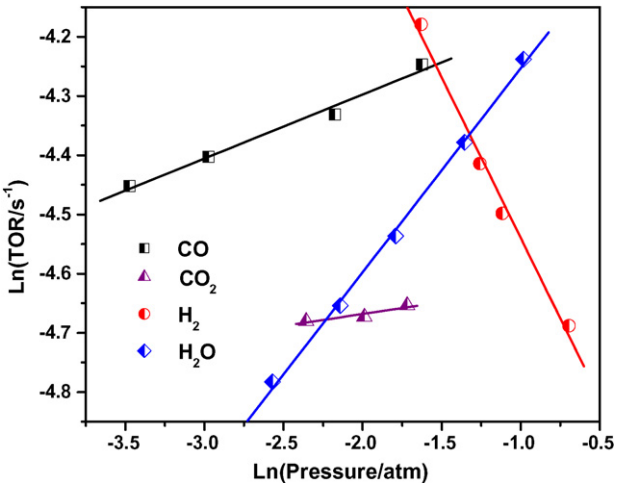

Fig. 2. Apparent reaction orders for CO, CO_2, H_2, and H_2O for 1% Pt/Al_2O_3 catalyst at 270 °C and 1 atm total pressure. Standard conditions were 7% CO, 8.5% CO_2, 22% H_2O, 37% H_2 and balance Ar. Order determination at standard conditions with each component varying in the range of 5–25% for CO, 5–30% for CO_2, 25–60% for H_2, and 10–46% for H_2O.

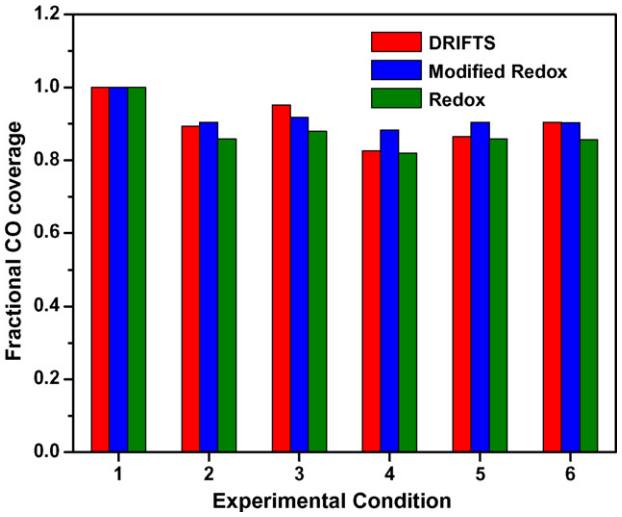

Fig. 3. Surface coverage of CO on 1.66% Pt/Al_2O_3 catalyst under various experimental conditions using DRIFTS and predicted from kinetic modeling. Experimental conditions from 1 to 6 were: 1—CO adsorption at 150 °C (6.8% CO and 93.2% N_2) and 2—standard WGS condition (300 °C, 6.8% CO, 8.5% CO_2, 37.3% H_2, 22% H_2O, 25.4% Ar). Other experiments at standard conditions and balance Ar except: 3—13.5% CO, 4—2.7% CO, 5—55.1% H_2, and 6—14% H_2.

catalysts tested in this study. This observation is consistent with the findings reported in previous studies [3,4,22–25]. Although there are reports in literature [14,26,27] on the deactivation of Pt/CeO_2 catalysts under WGS conditions, in this study, we did not observe any significant deactivation of our 1% Pt/CeO_2 catalyst. This apparent discrepancy is probably due to the different partial pressure and temperature ranges used in our study, and a direct comparison of our data with the ones in the literature should be carried out with care.

The concentration of H_2 and CO_2 during the WGS reaction is significant (as stated in Section 2) under conditions relevant to fuel reforming in fuel cell applications. Thus, the CO_2 and H_2 inhibition can be significant. Some of the previous studies [2,3,28] did not include CO_2 and H_2 in the feed stream. Nevertheless, CO_2 and H_2 are formed in the WGS reaction, but their effect on the forward WGS reaction rate was not considered. The reported reaction orders in earlier studies on $Pt–Al_2O_3$ [2] and $Pt–CeO_2$ [3] are different from the ones in our study. The reason for this difference can be that the reaction orders in [2,3] were not corrected for the presence of CO_2 and H_2 in the reactor. However, in some of the recent studies [22,24], the effect of CO_2 and H_2 on the forward WGS reaction rate was included. The apparent reaction orders and activation energy values from our study on 1% Pt/CeO_2 are similar to those reported by these authors [22,24] with the major difference being observed for the apparent reaction order for water. Our study and the study by Germani et al. [22] on CeO_2-based catalysts show an apparent reaction order for water close to 0.5, but the reported order from the study by Radhakrishnan et al. [24] is 0.85. This difference can be due to the effect of Re and the ceria-zirconia support used by Radhakrishnan et al. [24]. To compare the TOR values, the TOR values reported by Germani et al. [22] and Radhakrishnan et al. [24] were corrected to the standard conditions (6.8% CO, 8.5% CO_2, 22% H_2O, 37.3% H_2 and 25.4% Ar at 200 °C) in our study using the reported apparent reaction orders and activation energy [22,24]. The corrected TOR value from Radhakrishnan et al. [24] agrees well with the TOR value from our study on the 1% Pt/CeO_2 catalyst as both of these studies were carried out under similar reaction conditions. The corrected value from the study by Germani et al. [22] is approximately 1/7th of our TOR value on 1% Pt/CeO_2. This could be due to extrapolation involved in correcting the TOR value from their study [22]. In some other reports, the authors did not provide the kinetic parameters [23,28,29], and the apparent reaction orders and activation energy from our study were used to find the pre-exponential factor at their conditions. Assuming that this pre-exponential factor is the same under our conditions, we calculated the TOR for their catalysts under our standard conditions. The corrected TOR values from these studies [23,29] vary within an order of magnitude from the TOR value for our 1% Pt/CeO_2 catalyst. The extrapolation involved in correcting TOR values to our standard conditions can be the reason for this variation. Other studies in literature [30,31] were also considered for comparison. However, these studies were carried out at different temperatures than our study. At the temperatures of 100 °C [30] and 544 °C [31], the reaction kinetics could be different from the ones in our study. We have summarized the TOR values from literature corrected to the standard conditions in our study in Table 3.

We note from Table 3 that the apparent activation energies obtained for our 1% Pt/Al_2O_3 and 1% Pt/CeO_2 catalysts are similar (68 kJ mol^{-1} and 75 kJ mol^{-1}, respectively). Note that these apparent activation energies were measured in two different temperature ranges (250–315 °C for Pt/Al_2O_3 and 180–210 °C for Pt/CeO_2). The apparent reaction order for the forward reaction with respect to CO varies around zero for all Pt-based catalysts, from slightly positive (Pt/Al_2O_3) to slightly negative (Pt/CeO_2). To account for an almost zero order in CO with high binding strength and negative order in H_2 we had to include the well-known effect of decreasing binding strength of CO as the surface coverage is increased [32–35].

The forward reaction order for CO_2 is slightly negative and close to zero, which can be explained by a weak interaction of CO_2 with Pt. The apparent forward reaction order of H_2 close to −0.5 implies H_2 inhibition of the forward WGS. This suggests that after CO attains its saturation coverage, atomic hydrogen will be the dominant surface species on the remaining Pt sites. An increase in the partial pressure of hydrogen would result in an increase in the surface coverage of atomic hydrogen. This increase in the surface coverage of atomic hydrogen can inhibit the reaction by further lowering the available free Pt sites required for the activation of water. The apparent forward reaction order for H_2O is close to 1 for the alumina supported catalyst and close to 0.5 for the ceria supported catalyst. This difference in H_2O reaction order on alumina and ceria supported catalysts suggests that different reaction mechanisms may operate on these catalysts.

A clear difference in the reaction orders obtained for Cu-based catalysts [13] and Pt-based catalysts under the same reaction conditions is evident. The apparent forward reaction

Table 3
Literature values for kinetics of WGS reaction

Catalyst	Temperature[a] (°C)	TOR[b] ($\times 10^{-3}$ s^{-1})	E_a (kJ mol^{-1})	Reaction order				Reference
				CO	H_2O	CO_2	H_2	
1% Pt/Al_2O_3	285	1.3	68	0.06	1.0	−0.1	−0.44	This work
1% Pt/CeO_2	200	41.4	75	−0.03	0.44	−0.1	−0.38	This work
2% Pt/Al_2O_3	270	1.7	82	−0.21	0.75	–	–	[2]
1% Pt/CeO_2	240	24.0[c]	46	0	1	–	–	[3]
0.9% Pt/Al_2O_3	100	–	–	0.02	0.55	–	−0.22	[30]
0.4% Pt/Al_2O_3	544	–	39	0.45	0.37	0.0	−0.73	[31]
1.4% Pt–8.3% CeO_2/Al_2O_3	260	5.9[d]	86	0.13	0.49	−0.12	−0.45	[22]
1% Pt–12% CeO_2/Al_2O_3	–	108	–	–	–	–	–	[23]
5% Pt/CeO_2	–	1.10	–	–	–	–	–	[29]
2% Pt–1% Re/CeO_2–ZrO_2	210–240	30.5	71	−0.05	0.85	−0.05	−0.32	[24]

[a] Temperature at which the reaction order measurements were carried out.
[b] TOR (per surface Pt atom) for overall reaction corrected to 200 °C, 1 atm total pressure, 7% CO, 8.5% CO_2, 22% H_2O, 37% H_2, and 25.5% Ar.
[c] The value estimated from Fig. 1 in Ref. [3].
[d] Calculated at our conditions from the analytical expression provided.

orders for industrial Cu–ZnO–Al_2O_3 catalyst measured [13] at 200 °C were as follows: CO, 0.8; H_2O, 0.8; CO_2, −0.7; H_2, −0.8. The different values for Cu-based and Pt-based catalysts suggest that the reaction mechanisms or rate determining steps (RDS) on these catalysts are distinct. The redox mechanism was probably prevalent under the conditions in which Cu-based catalysts were investigated [13]. Although the redox mechanism is not probable for Pt, we wanted to test if this model could be fitted to the data with physically relevant parameters.

4.2. Reaction kinetic modeling

A power rate law expression is useful for the design of reactors (Table 2). It also serves as an indication of the prevalent reaction mechanism. Extracting a plausible reaction mechanism from a power-rate law is possible in many cases [36]. However, from the apparent activation energy and reaction orders determined in Table 2, we could not infer the reaction steps conclusively. To study the WGS mechanism on these catalysts, we carried out a kinetic analysis where the elementary steps are proposed and the resulting system of equations is solved simultaneously. This approach is described in detail by Dumesic et al. [37] and for the WGS reaction by Lund [38]. The reaction mechanism considered for kinetic analysis of Pt/Al_2O_3 data is based on the redox mechanism proposed by Ovesen et al. [39,40]. The steps considered in our study are as follows (* is a free/empty site):

$$H_2O + {}^* \rightleftarrows H_2O^* \quad (1)$$

$$H_2O^* + {}^* \rightleftarrows OH^* + H^* \quad (2)$$

$$OH^* + {}^* \rightleftarrows O^* + H^* \quad (3)$$

$$2H^* \rightleftarrows H_2 + 2^* \quad (4)$$

$$CO + {}^* \rightleftarrows CO^* \quad (5)$$

$$CO^* + O^* \rightleftarrows CO_2{}^* + {}^* \quad (6)$$

$$CO_2{}^* \rightleftarrows CO_2 + {}^* \quad (7)$$

The mechanism (1)–(7) can be seen as a combination of surface oxidation, $H_2O + {}^* \rightleftarrows H_2 + O^*$ (obtained by combining steps (1)–(4)), and surface reduction, $CO + O^* \rightleftarrows CO_2 + {}^*$ (obtained by combining steps (5)–(7)). The sequence of elementary steps (1)–(7) is called a ''Redox mechanism''. The steps in the methanation route were not considered although Pt-based catalysts show methanation at higher temperatures (>300 °C) [41]. This is justified because we did not observe any methanation for 1% Pt/Al_2O_3 and 1% Pt/CeO_2 catalysts under the reaction conditions of this study. Ovesen et al. [39,40] considered one more step of OH disproportionation ($OH^* + OH^* \rightleftarrows H_2O^* + O^*$) in their kinetic model. It is unclear from the literature whether the OH disproportionation reaction as written above is an elementary step or not [42,43]. Hence, we did not consider this step in our kinetic model.

The set of seven steps of the redox mechanism was chosen for the kinetic modeling. The activation energies and the pre-exponential factors for these elementary steps are the kinetic parameters in the model. Following Lund [38], the binding strengths of the various surface intermediates were also chosen as parameters in the model. The binding strengths were used to determine the heat of reaction for surface reactions. The initial guesses of kinetic parameters were taken from the values provided in the literature [44–46] and from our own periodic density functional theory (DFT) calculations.

We assumed that the reactor operates as a plug-flow reactor. Therefore, in the kinetic model, five ordinary differential equations for gas flow rates versus catalyst mass were solved. These differential equations were combined with six steady-state equations for the fractional coverages of surface species (CO^*, $CO_2{}^*$, H^*, H_2O^*, OH^*, and O^*) and one site balance equation. The equation solving and the parameter fitting was performed using Athena Visual Workbench engineering software [47].

4.2.1. Seven-step redox mechanism

When we include the coverage-dependence of CO binding strength in the kinetic model based on the seven-step redox mechanism, we can explain the high CO coverage and the close

to zero apparent forward reaction order with respect to CO. The relationship between CO surface coverage and its binding strength was modeled using a linear relationship as: $BS_{CO}(\theta_{CO^*}) = BS_{CO}(\theta_{CO^*} \rightarrow 0\,ML) - 39\theta_{CO^*}$, as derived from our DRIFTS study as well as using the expression in Refs. [32–34]:
$BS_{CO}(\theta_{CO^*}) = BS_{CO}(\theta_{CO^*} = 0.25\,ML) - 0.63\exp(4.79\,\theta_{CO^*})$.
In this study, we modified the expression in Refs. [32–34] to
$BS_{CO}(\theta_{CO^*}) = BS_{CO}(\theta_{CO^*} \rightarrow 0\,ML) - 0.63\exp(4.79\,\theta_{CO^*})$.
Both of these relationships explain the experimental kinetic data (TOR) with $R^2 = 0.97$. The parity plot comparing calculated TOR versus the experimentally observed TOR for the 1.66% Pt/Al_2O_3 catalyst is shown in Fig. 4 ($R^2 = 0.97$). The plot of residuals versus the predicted TOR (Fig. 5) also confirms the goodness of the fit. The residual values are small as compared to calculated TOR values (<10%) and the plot (Fig. 5) shows a random distribution of residuals, confirming the goodness of the fit.

We also developed the kinetic model based on the seven-step redox mechanism without including the coverage-dependence of CO binding strength. This model explains the kinetic data on the alumina-supported catalysts reasonably well with R^2 of 0.98 (results not shown here). However, the predicted fractional coverage of CO was of the order of 10^{-2} to 10^{-4} ML, while the most abundant surface intermediate was H^* (coverage of ~0.5 ML). This is contrary to the experimental observations that CO adsorbs strongly on Pt and thus should yield close to saturation coverage on the Pt surface [30,35]. When all the parameters in this model were estimated (except the binding energy of CO, which was kept fixed to 100 kJ mol^{-1} to ensure significant surface coverage of CO), the calculated CO order was negative (~−0.45), inconsistent with the experimentally measured CO reaction order of 0.1. Despite the fit with R^2 of 0.97 obtained for experimental kinetic data, we conclude that this model could not capture the underlying physical phenomenon. Thus, the kinetic model based on the seven-step redox mechanism without the coverage dependence of CO binding strength cannot explain the close to zero CO reaction order for a CO surface coverage close to saturation.

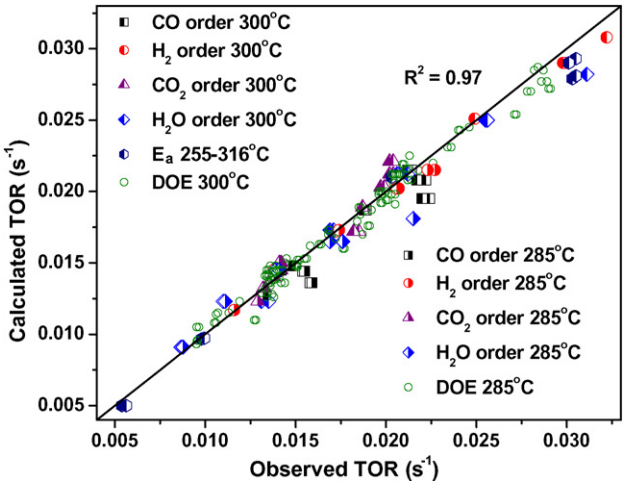

Fig. 4. Plot of calculated vs. observed TOR. 1.66% Pt/Al_2O_3 catalyst operated between 255 °C and 316 °C, 1 atm total pressure (284 points total) using the redox mechanism. DOE indicates the experiments from central composite design.

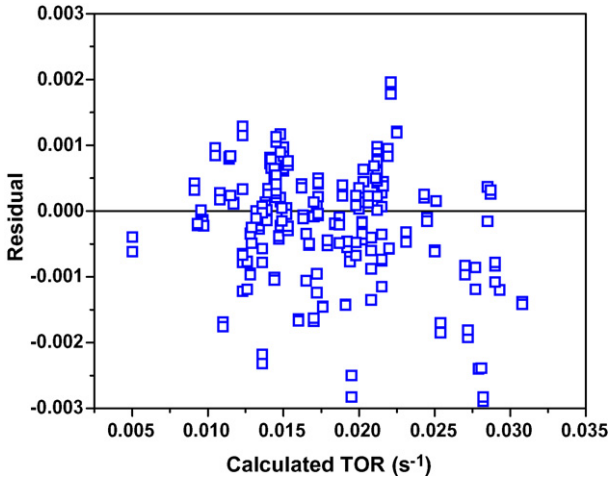

Fig. 5. Residual plot for 1.66% Pt/Al_2O_3 operated between 255 °C and 316 °C and 1 atm total pressure using the redox mechanism.

We mentioned earlier that when the coverage dependence of the CO binding strength was included, a kinetic model based on the seven-step redox mechanism could explain the experimental kinetic data. In this kinetic model, due to saturation coverage of CO and high barriers for complete dissociation of water to form surface oxygen and hydrogen on Pt (85 kJ mol^{-1} for step (2) and 102 kJ mol^{-1} for step (3)) [48], the surface coverages of OH^* and O^* will be low. At these coverages, the CO_2 production pathway involving CO^* and OH^* would compete with reaction pathway involving CO^* and O^*. This phenomenon is explicitly considered in the modified redox mechanism.

4.2.2. Modified redox mechanism

It is suggested in the literature [49,50] that there are pathways for oxidation of CO to CO_2 other than surface oxidation ($CO^* + O^* \rightleftarrows CO_2{}^* + {}^*$). We considered the "direct CO_2 production pathway" from [49] by modifying the redox mechanism. In this modified pathway, step (3) from the seven-step redox mechanism is not considered while the step (6) is modified to $CO^* + OH^* \rightleftarrows CO_2{}^* + H^*$.

In the kinetic model based on this modified redox mechanism, we accounted for the coverage-dependence of the CO binding strength. The optimal estimates of parameters obtained by fitting the experimental data using the modified redox mechanism are listed in Table 4. The parity plot of the calculated TOR versus observed TOR for the 1.66% Pt/Al_2O_3 catalyst using this modified redox mechanism is shown in Fig. 6. The residual values (Fig. 7) are small as compared to calculated TOR values (<10%).

In conclusion, although the seven-step redox and modified redox mechanisms can explain the kinetic data quantitatively, further information about the surface intermediates and their relative coverages is required to distinguish between the two mechanisms.

Table 4
List of parameters used in the kinetic modeling of 1.66% Pt/Al_2O_3 data using modified redox mechanism

Parameters[a]	Optimal estimates[a]
BS(CO^*)[b]	117
BS(CO_2^*)	23
BS(H^*)	251
BS(H_2O^*)	77
BS(OH^*)	267
$E_a(1)$	0
$E_a(2)$	37
$E_a(3)$	30
$E_a(4)$	2
$E_a(5)$	61
$E_a(6)$	12
$\ln[k_0(1)]$	8
$\ln[k_0(2)]$	24
$\ln[k_0(3)]$	24
$\ln[k_0(4)]$	14
$\ln[k_0(5)]$	24
$\ln[k_0(6)]$	23

[a] BS implies binding strength (in kJ mol^{-1}), $E_a(I)$ denotes activation energy for step (I) (in units of kJ mol^{-1}), and $k_0(I)$ denotes pre-exponential factor for step (I) (in units of s^{-1} or atm^{-1} s^{-1}) [*Note*: I = 1–6 is same sequence as the steps in modified redox mechanism from Section 4.3.].

[b] Dependence of binding strength of CO on the surface coverage is taken into account using the following expression: $BS_{CO}(\theta_{CO^*}) = BS_{CO}(\theta_{CO^*} \rightarrow 0\,ML) - 0.63\exp(4.79\,\theta_{CO^*})$.

4.3. DRIFTS study on Pt/Al_2O_3 catalysts

The DRIFTS study on the 1.66% Pt/Al_2O_3 catalyst was carried out to estimate the changes in surface coverage of CO under relevant experimental conditions. This was done by comparing the area under the peaks in DRIFTS spectra corresponding to adsorbed CO under various WGS conditions with the one obtained by exposing the catalyst to 6.8% CO in N_2 at 150 °C (saturation coverage). As shown in Fig. 3, the surface coverage of CO under various reaction conditions is close to the saturation coverage of CO.

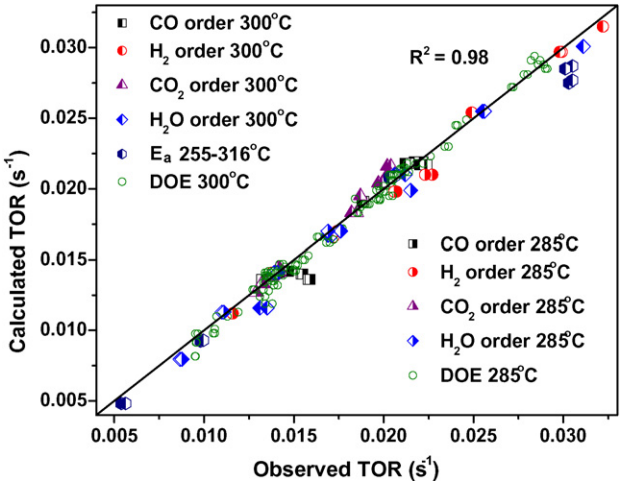

Fig. 6. Plot of calculated vs. observed TOR for 1.66% Pt/Al_2O_3 catalyst operated between 255 °C and 316 °C, 1 atm total pressure (284 points total) using the modified redox mechanism. DOE indicates the experiments from central composite design.

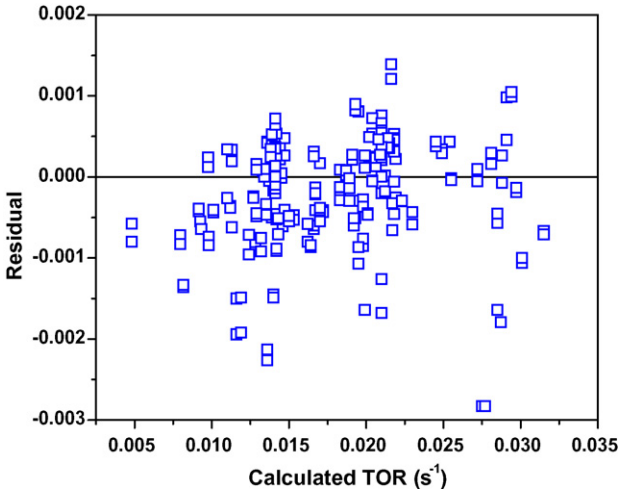

Fig. 7. Residual plot for 1.66% Pt/Al_2O_3 operated between 255 °C and 316 °C and 1 atm total pressure using the modified redox mechanism.

The coverage-dependence of the heat of adsorption of CO was observed from our DRIFTS study. The DRIFTS spectra were measured at different temperatures under 6.8% CO in N_2 and the relative CO coverage was estimated at each temperature. In our study, the heat of adsorption of CO was obtained for coverages from 0.36 to 1. Using the approach explained by Chafik et al. [35], the heat of adsorption of CO was estimated at each CO coverage. In this approach [35], it was assumed that the integrated absorption intensity of the adsorbed CO was independent of temperature and coverage. It was also assumed that the Langmuir's model for adsorption without dissociation can be used and the equilibrium constant for adsorption can be calculated by statistical thermodynamics assuming the loss of all three translational degrees of freedom [35]. The estimated values for heat of adsorption of CO range from 121 kJ mol^{-1} (θ_{CO} = 0.36) to 100 kJ mol^{-1} (θ_{CO} = 1) for the 1.66% Pt/Al_2O_3 catalyst. The decrease in the heat of adsorption of CO as a linear function of its surface coverage fits the data with R^2 of 0.97. A linear decrease in heat of adsorption of CO with increasing coverage was also observed in earlier experimental studies [35,51].

From kinetic modeling, we have optimal estimates of kinetic parameters for the seven-step redox mechanism and modified redox mechanism. These optimal estimates of kinetic parameters were used to predict the coverages under the various reaction conditions investigated using DRIFTS. In Fig. 3, we have compared the surface coverage of CO measured using DRIFTS with the predicted coverage. It is evident from Fig. 3 that both mechanisms explain the DRIFTS measurements qualitatively.

In the previous section, we showed that the seven-step redox mechanism without coverage-dependence of CO binding strength could explain the kinetic data. However, this model could not capture the saturation surface coverage of CO under WGS conditions. We have also shown that the redox-type mechanisms accounting for coverage-dependence of CO

binding strength can explain the kinetic data quantitatively. Hence, the reaction kinetic data and DRIFTS measurements are not sufficient to elucidate the nature of reaction intermediates in the WGS mechanism or to distinguish between the various redox-type mechanisms and further information such as isotopic transient kinetic data is necessary. This data will provide the rate of formation of possible reaction intermediates, which upon comparison with the rate of the WGS reaction will help identify the dominant WGS mechanism on the Pt/Al_2O_3 catalyst under different conditions.

4.4. WGS reaction mechanism on ceria supported Pt catalysts

The redox mechanisms (Section 4.2) proposed for the Pt/Al_2O_3 catalysts may not explain the kinetic data on Pt/CeO_2 due to different reaction orders. The differences in reaction orders and an increase in TOR by a factor of 30 by addition of CeO_2 point to a different WGS mechanism on ceria-based catalysts than on alumina-based catalysts. This promotional effect of ceria can either be rationalized by a change in the rate-determining step for the redox mechanism or by a different reaction mechanism on ceria or both. Several groups have invoked a redox mechanism for the WGS reaction on ceria-supported catalysts [3,4,52]. It is believed that the ceria support plays an important role in the redox mechanism by providing sites for water activation [4]. Some other groups have proposed an associative reaction mechanism for ceria-based catalysts [9–12]. Shido and Iwasawa [9,10] proposed an associative reaction mechanism based on their FTIR studies on CeO_2 and Rh-doped CeO_2. Recently, Jacobs et al. [11,12] observed from their isotope switching experiments monitored using DRIFTS that the water gas shift mechanism over metal promoted ceria occurs through a formate intermediate as suggested by Shido and Iwasawa. In another study, Goguet et al. [27,53] showed that instead of formates, surface carbonates were the main reaction intermediates on $Pt–CeO_2$ under reverse WGS (RWGS) conditions using steady-state isotopic transient kinetic analysis (SSITKA) techniques. In a more recent study, Meunier et al. [54] reported that a switchover from a non-formate to a formate-based mechanism could take place over a narrow temperature range (as low as 60 K) over a 2% Pt/CeO_2 catalyst. This implies that the WGS reaction mechanism on ceria-supported catalysts can be a function of the reaction conditions. This study also suggested that the same surface species (formate) can be the spectator species under certain reaction conditions and can be the main reaction intermediate under different reaction conditions. In the modified redox mechanism considered in this study, we could not determine the exact nature of the reaction intermediate formed from CO^* and OH^*. The reaction intermediate can be for example the formate ($HCOO^{**}$) species or the carboxyl ($COOH^*$) species. Thus, further investigation of the $Pt–Al_2O_3$ and $Pt–CeO_2$ catalysts using steady state isotopic transient kinetic analysis under reaction conditions is necessary.

5. Summary

We have reported the WGS reaction rates, apparent activation energy, and apparent reaction orders for Pt/Al_2O_3 and Pt/CeO_2 catalysts at conditions relevant to fuel processing for fuel cell applications. For Pt/Al_2O_3 catalysts, the reaction order measured in the range of 270–315 °C is close to zero for CO and CO_2, about 1.0 for H_2O and −0.5 for H_2. Apparent reaction orders for the Pt/CeO_2 catalyst are the same as those observed for the Pt/Al_2O_3 catalyst except the order with respect to H_2O (∼0.5). On the basis of the TOR, ceria is a strong promoter for Pt based WGS catalysts.

We showed that the two distinct kinetic models, the seven-step redox mechanism as well as the modified redox mechanism, explain the quantitative experimental reaction kinetic data. It was not possible to choose a kinetic model or elucidate the nature of reaction intermediates in these mechanisms using only the kinetic data presented here. Thus, further isotopic transient kinetic data is needed to elucidate the reaction pathway. It is also important to note that the model captured the close to saturation coverages of CO and the close to zero reaction order of CO only when the coverage dependence of the binding strength of CO was explicitly included in the kinetic model.

Acknowledgements

Support for this research was provided by the U.S. Department of Energy, Office of Basic Energy Sciences, through the Catalysis Science Grant no. DE-FG02-03ER15466. We are grateful to Dr. David G. Taylor, K.M. Lee, P. Figaro, and Dr. G. Zhu, for assistance in building the experimental setup. The authors thank K.M. Lee for collecting experimental data on the 1% $Pt–Al_2O_3$ sample.

References

[1] R. Farrauto, S. Hwang, L. Shore, W. Ruettinger, J. Lampert, T. Giroux, Y. Liu, O. Ilinich, Ann. Rev. Mater. Res. 33 (2003) 1.
[2] D.C. Grenoble, M.M. Estadt, D.F. Ollis, J. Catal. 67 (1981) 90.
[3] T. Bunluesin, R.J. Gorte, G.W. Graham, Appl. Catal. B 15 (1998) 107.
[4] S. Hilaire, X. Wang, T. Luo, R.J. Gorte, J. Wagner, Appl. Catal. A 258 (2004) 271.
[5] D. Andreeva, V. Idakiev, T. Tabakova, L. Ilieva, P. Falaras, A. Bourlinos, A. Travlos, Catal. Today 72 (2002) 51.
[6] M. Niwa, J.H. Lunsford, J. Catal. 75 (1982) 302.
[7] W.S. Epling, L.E. Campbell, A. Yezerets, N.W. Currier, J.E. Parks, Catal. Rev. Sci. Eng. 46 (2004) 163.
[8] J. Barbier Jr., D. Duprez, Appl. Catal. B 4 (1994) 105.
[9] T. Shido, Y. Iwasawa, J. Catal. 141 (1993) 71.
[10] T. Shido, Y. Iwasawa, J. Catal. 136 (1992) 493.
[11] G. Jacobs, P.M. Patterson, U.M. Graham, D.E. Sparks, B.H. Davis, Appl. Catal. A 269 (2004) 63.
[12] G. Jacobs, S. Khalid, P.M. Patterson, D.E. Sparks, B.H. Davis, Appl. Catal. A 268 (2004) 255.
[13] N.A. Koryabkina, A.A. Phatak, W.F. Ruettinger, R.J. Farrauto, F.H. Ribeiro, J. Catal. 217 (2003) 233.
[14] X. Liu, W. Ruettinger, X. Xu, R. Farrauto, Appl. Catal. B 56 (2005) 69.
[15] J.E. Benson, M. Boudart, J. Catal. 4 (1965) 704.
[16] J.E. Benson, H.S. Hwang, M. Boudart, J. Catal. 30 (1973) 146.
[17] W. Ruettinger, X. Liu, R.J. Farrauto, Appl. Catal. B 65 (2006) 135.

[18] D.C. Montgomery, G.C. Runger, Applied Statistics and Probability for Engineers, Wiley, New York, 2003.
[19] W.N. Delgass, G.L. Haller, R. Kellerman, J.H. Lunsford, Spectroscopy in Heterogeneous Catalysis, Academic Press, New York, 1979.
[20] P. Kubelka, F. Munk, Zeitschrift fur technische Physik 12 (1931) 593.
[21] H. Bohlbro, An Investigation on the Kinetics of the Conversion of Carbon Monoxide with Water Vapour over Iron Oxide Based Catalysts, Gjellerup, Copenhagen, 1969.
[22] G. Germani, P. Alphonse, M. Courty, Y. Schuurman, C. Mirodatos, Catal. Today 110 (2005) 114.
[23] G. Kolb, H. Pennemann, R. Zapf, Catal. Today 110 (2005) 121.
[24] R. Radhakrishnan, R.R. Willigan, Z. Dardas, T.H. Vanderspurt, Appl. Catal. B 66 (2006) 23.
[25] Q. Fu, H. Saltsburg, M. Flytzani-Stephanopoulos, Science 301 (2003) 935.
[26] J.M. Zalc, V. Sokolovskii, D.G. Löffler, J. Catal. 206 (2002) 169.
[27] A. Goguet, F. Meunier, J.P. Breen, R. Burch, M.I. Petch, A.F. Ghenciu, J. Catal. 226 (2004) 382.
[28] P. Panagiotopoulou, D.I. Kondarides, J. Catal. 225 (2004) 327.
[29] C.M.Y. Yeung, K.M.K. Yu, Q.J. Fu, D. Thompsett, M.I. Petch, S.C. Tsang, J. Am. Chem. Soc. 127 (2005) 18010.
[30] R. He, R.R. Davda, J.A. Dumesic, J. Phys. Chem. B 109 (2005) 2810.
[31] C.W. Lam, M.S. Stacey, D.L. Trimm, Chem. Eng. Sci. 36 (1981) 224.
[32] A.A. Gokhale, S. Kandoi, J.P. Greeley, M. Mavrikakis, J.A. Dumesic, Chem. Eng. Sci. 59 (2004) 4679.
[33] S. Kandoi, J. Greeley, M. Sanchez-Castillo, S. Evans, A. Gokhale, J. Dumesic, M. Mavrikakis, Top. Catal. 37 (2006) 17.
[34] L. Grabow, Y. Xu, M. Mavrikakis, Phys. Chem. Chem. Phys. 8 (2006) 3369.
[35] T. Chafik, O. Dulaurent, J.L. Gass, D. Bianchi, J. Catal. 179 (1998) 503.
[36] M. Boudart, G. Djéga-Mariadassou, Kinetics of Heterogeneous Catalytic Reactions, Princeton University Press, Princeton, NJ, 1984.
[37] J.A. Dumesic, D.F. Rudd, L.M. Aparicio, J.E. Rekoske, A.A. Treviño, The Microkinetics of Heterogeneous Catalysis, American Chemical Society, Washington, 1993.
[38] C.R.F. Lund, Ind. Eng. Chem. Res. 35 (1996) 2531.
[39] C.V. Ovesen, P. Stoltze, J.K. Nørskov, C.T. Campbell, J. Catal. 134 (1992) 445.
[40] C.V. Ovesen, B.S. Clausen, B.S. Hammershøi, G. Steffensen, T. Askgaard, I. Chorkendorff, J.K. Nørskov, P.B. Rasmussen, P. Stoltze, P. Taylor, J. Catal. 158 (1996) 170.
[41] O. Korotkikh, W.F. Ruettinger, R.J. Farrauto, US Patent 6,562,315 B2, Engelhard Corporation, 2003.
[42] K. Bedürftig, S. Völkening, Y. Wang, J. Wintterlin, K. Jacobi, G. Ertl, J. Chem. Phys. 111 (1999) 11147.
[43] A. Michaelides, P. Hu, J. Am. Chem. Soc. 123 (2001) 4235.
[44] P. Aghalayam, Y.K. Park, N. Fernandes, V. Papavassiliou, A.B. Mhadeshwar, D.G. Vlachos, J. Catal. 213 (2003) 23.
[45] M.J. Hei, H.B. Chen, J. Yi, Y.J. Lin, G. Wei, D.W. Liao, Surf. Sci. 417 (1998) 82.
[46] I. Barin (Ed.), Thermochemical Data of Pure Substances, VCH, Weinheim, 1993.
[47] W.E. Stewart, M. Caracotsios, J.P. Sorensen, AIChE J. 38 (1992) 641.
[48] S. Kandoi, A.A. Gokhale, L.C. Grabow, J.A. Dumesic, M. Mavrikakis, Catal. Lett. 93 (2004) 93.
[49] A.B. Mhadeshwar, D.G. Vlachos, J. Phys. Chem. B 108 (2004) 15246.
[50] A.B. Mhadeshwar, D.G. Vlachos, Catal. Today 105 (2005) 162.
[51] R.W. McCabe, L.D. Schmidt, Surf. Sci. 66 (1977) 101.
[52] Y. Li, Q. Fu, M. Flytzani-Stephanopoulos, Appl. Catal. B 27 (2000) 179.
[53] A. Goguet, F.C. Meunier, D. Tibiletti, J.P. Breen, R. Burch, J. Phys. Chem. B 108 (2004) 20240.
[54] F.C. Meunier, D. Tibiletti, A. Goguet, S. Shekhtman, C. Hardacre, R. Burch, Catal. Today (2006), doi:10.1016/j.cattod.2006.10.003.